ADVANCED FUNCTIONAL MATERIALS
www.afm-journal.de

Controllable Broadband Absorption in the Mixed Phase of Metamagnets

Matej Pregelj, Oksana Zaharko, Andrej Zorko, Matjaž Gomilšek, Oles Sendetskyi, Axel Günther, Mykhaylo Ozerov, Sergei A. Zvyagin, Hubertus Luetkens, Christopher Baines, Vladimir Tsurkan, and Alois Loidl*

Materials with broad absorption bands are highly desirable for electromagnetic filtering and processing applications, especially if the absorption can be externally controlled. Here, a new class of broadband-absorption materials is introduced. Namely, layered metamagnets exhibit an electromagnetic excitation continuum in the magnetic-field-induced mixed ferro- and antiferromagnetic phase. Employing a series of complementary experimental techniques involving neutron scattering, muon spin relaxation, specific heat, ac and dc magnetization measurements, and electron magnetic resonance, a detailed magnetic phase diagram of $Cu_3Bi(SeO_3)_2O_2Br$ is determined and it is found that the excitations in the mixed phase extend over at least ten decades of frequency. The results, which reveal a new dynamical aspect of the mixed phase in metamagnets, open up a novel approach to controllable microwave filtering.

1. Introduction

The existence of magnetic excitation continua is intriguing from a theoretical as well as from an application point of view. In condensed matter physics they are typically associated with unconventional fractional excitations,[1–6] nontrivial scale-invariant quantum excitations at quantum critical points,[7–12] and nonresonant absorption in superconductors.[13] In the context of applications, broadband microwave absorption is highly desirable in microwave filters,[14] signal-to-noise enhancers, optical signal processing,[15–17] electromagnetic interference shielding,[18,19] etc. Most of these applications are based on conducting materials, even though normal metals possess relatively narrow absorption ranges (typically 100–1000 MHz).[18] Hence, composite carbon-based materials,[19–21] which extend the absorption range from hundreds of kHz up to hundreds of GHz,[18] and multilayer magnetic structures that cover the range between several GHz and several THz[22–26] are being developed. However, none of these materials allow for external control of their absorption properties, e.g., by the electric or the magnetic field.

A class of materials that could allow for a controllable (on-demand) broadband absorption are metamagnets. These systems are, typically, highly anisotropic and, as a function of the external magnetic field, undergo a first-order phase transition from a state with low magnetization to a state with high magnetization.[27] Prominent examples are layered metamagnets with perpendicular anisotropy, where ferromagnetic (FM) layers are antiferromagnetically (AFM) aligned. Such systems are not affected by magnetic fields perpendicular to the layers until the applied field becomes comparable to the AFM interlayer interaction, when a first-order transition to an FM structure occurs. If a finite demagnetization field is present, the high-field FM phase is reached through a "mixed phase," existing in a finite range of fields. In this phase, AFM and FM orders coexist.[27–30] There are numerous possible arrangements of FM and AFM domains,[29,30] and consequently a very rich excitation spectrum can be anticipated. Up to now, studies of the mixed phase have almost exclusively been restricted to ac susceptibility measurements and thus to a frequency range of 0.1–100 kHz.[31–35] Therefore, the intriguing dynamics of the mixed phase have remained elusive.

In this paper, we focus on the recently discovered layered metamagnet $Cu_3Bi(SeO_3)_2O_2Br$, with kagome-like Cu layers stacked along the *c*-axis.[36] At $T_N = 27.4$ K, the system develops

Dr. M. Pregelj, Dr. A. Zorko, M. Gomilšek
Jožef Stefan Institute
Jamova c. 39, 1000 Ljubljana, Slovenia
E-mail: matej.pregelj@ijs.si
Dr. O. Zaharko, O. Sendetskyi,
Dr. H. Luetkens, C. Baines
Laboratory for Neutron Scattering and Laboratory for Micro- und Nanotechnology and Laboratory for Muon-Spin Spectroscopy
Paul Scherrer Institut
CH-5232 Villigen, Switzerland
A. Günther, Dr. V. Tsurkan, Prof. A. Loidl
Experimental Physics V
Center for Electronic Correlations and Magnetism
University of Augsburg
86135 Augsburg, Germany
Dr. M. Ozerov, Dr. S. A. Zvyagin
Dresden High Magnetic Field Laboratory (HLD)
Helmholtz-Zentrum Dresden-Rossendorf
01328 Dresden, Germany
Dr. V. Tsurkan
Institute of Applied Physics
Academy of Sciences of Moldova
MD-2028 Chisinau, Republic of Moldova

DOI: 10.1002/adfm.201500702

the AFM order of alternating FM (*ab*) layers, which in a magnetic field of B_C(10 K) ≈ 0.8 T that is applied perpendicular to the layers undergoes a metamagnetic transition.[37] This convenient field and temperature range allow for the use of various complementary experimental techniques to investigate its magnetic excitations in a very broad frequency range. Employing neutron scattering, muon spin relaxation (μSR), specific heat, ac and dc magnetization, and electron magnetic resonance (EMR), we precisely map the mixed phase in the magnetic phase diagram and trace its dynamics in the range from 100 Hz to 480 GHz. Our results show that the dynamics pertinent to the mixed phase extend over the whole frequency range, i.e., at least over ten decades of frequency—a sign of a scale invariance characteristic of enigmatic entangled-quantum-critical states.[7–12] Alternatively, such an extremely broad frequency range suggests that several different fluctuation channels have to be active simultaneously as only a single one would result in a much narrower frequency spectrum.[38] The observed behavior highlights a new aspect of layered metamagnets, making them highly attractive for testing theories, as well as for applications, where magnetic-field control of broadband absorption is desired.

2. Results

2.1. Coexistence of the FM and AFM Phases

To investigate the magnetic order in the vicinity of the metamagnetic transition, we performed neutron diffraction measurements in magnetic fields applied along the *c*-axis. The temperature dependence of the intensities of the FM (2 –1 0) and the AFM (2 –1 0.5) reflections measured at several magnetic field strengths clearly shows that the two reflections coexist in a narrow field range (**Figure 1**a). A complementary field dependence measured at 2 K reveals that the AFM reflection persists up to $B_{C2}(T = 2\ \text{K}) \approx 0.84$ T, whereas the FM one emerges already at $B_{C1}(T = 2\ \text{K}) \approx 0.76$ T (Figure 1b). Importantly, the widths of the peaks do not change until their intensity is almost completely suppressed (Figure 1c), which evidences that both coexisting orders within the mixed FM/AFM phase are well correlated, i.e., the correlation lengths of both orders exceed the instrumental resolution along the *b*- and *c*-axes, respectively (see the Experimental Section). Finally, a comparison of *l*-scans (not shown) measured between (0 2 0.5) and (0 2 1) at 0.79 T and 2 K (where AFM and FM orders coexist) with the same scans measured at 35 K (above T_N) shows no sign of diffuse magnetic scattering and thus excludes potential incommensurate correlations between the *ab* FM layers, i.e., along the *c*-axis.

2.2. Development of the Demagnetization Field

Neutron scattering experiments clearly demonstrate the coexistence of the AFM and FM orders in a certain temperature-field region (Figure 1). However, the short time scale of the neutron experiment does not allow us to differentiate between a frozen phase-separated state and a dynamical/fluctuating state. Hence, we resort to μSR, a local-probe technique that can resolve whether local magnetic fields B_μ are static on time scales of $< 2\pi/(\gamma_\mu B_\mu) \approx 10^{-7}$ s (≈10 MHz), where $\gamma_\mu = 2\pi \times 135.5$ MHz T^{-1}.[39] The

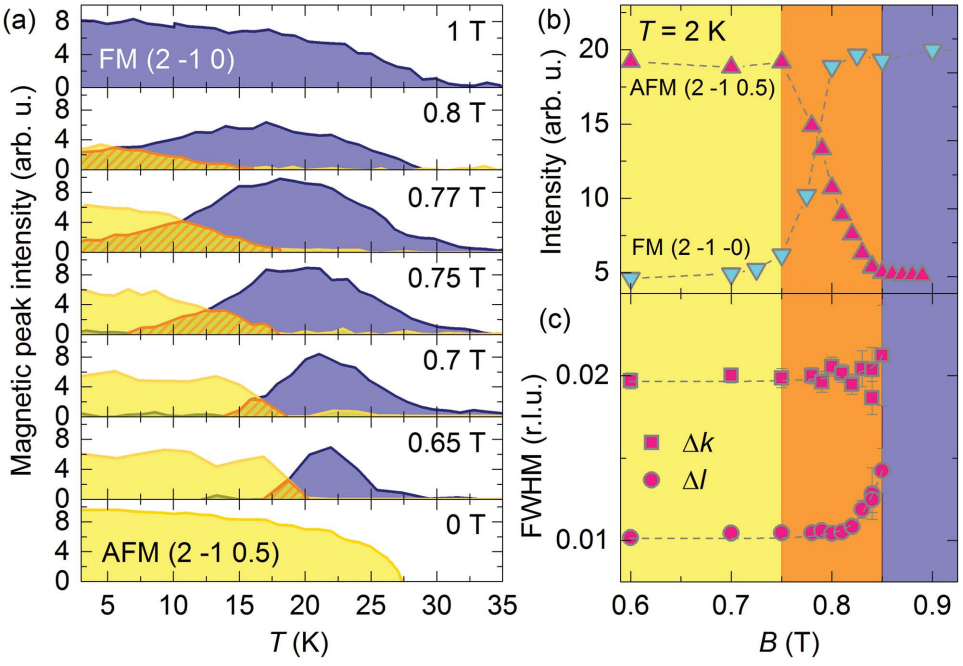

Figure 1. a) Temperature dependencies of the FM (blue) and AFM (yellow) reflections in neutron diffraction, corresponding to high- and low-field magnetic phases, respectively, measured in a magnetic field applied along the *c*-axis. Field dependence of b) intensities and c) widths of the AFM magnetic peak measured at 2 K. The latter do not change (they are limited by instrumental resolution) until the peak almost completely disappears, indicating that both orders are well correlated in the mixed phase.

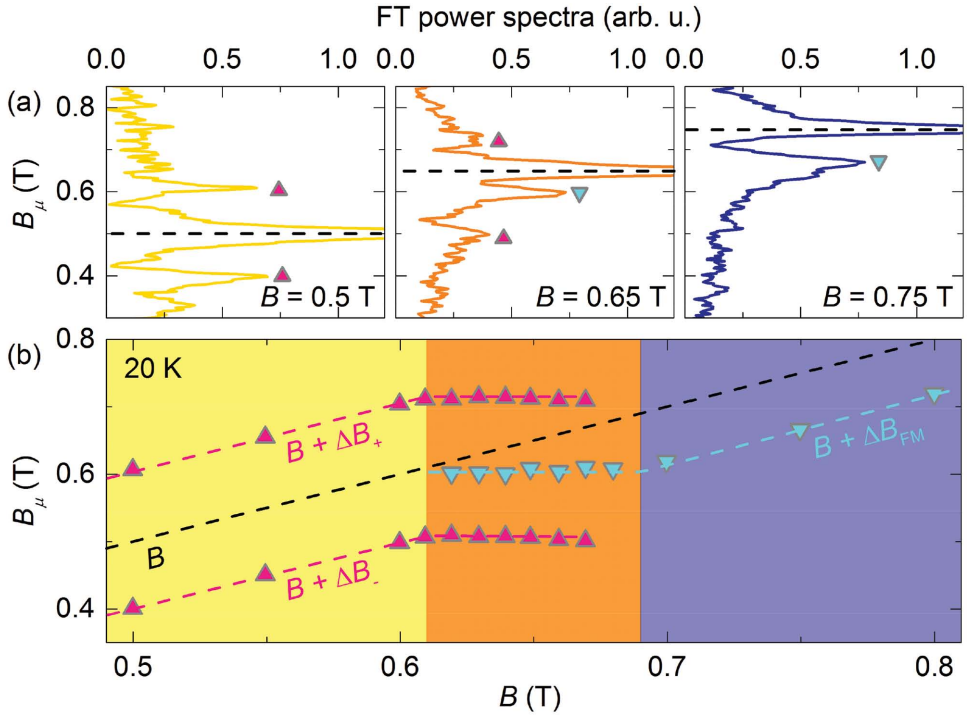

Figure 2. a) Fourier transform power spectra of muon spin polarization at 20 K plotted as a function of the applied magnetic field. b) Local magnetic fields at the muon sites as a function of the applied magnetic field. The latter has no effect on the local fields in the mixed phase, which is a direct consequence of the demagnetization effect.

experiments were performed at several magnetic fields strengths (**B**||*c*) at 20 K, focusing on the mixed phase between $B_{C1}(T = 20\ \text{K}) = 0.61(1)$ T and $B_{C2}(T = 20\ \text{K}) = 0.69(1)$ T.[37] At $B = 0.5$ T, i.e., well below $B_{C1}(T = 20\ \text{K})$, a Fourier transformation of the time-dependent muon polarization perpendicular to the applied field clearly reveals three spectral components, corresponding to three distinct resonant fields (**Figure 2**a). The strongest signal at $B_\mu = B$ corresponds to the muons that stop in the Ag sample holder (≈50%), where local fields match the applied external field B. The other two signals are symmetrically displaced from the main line, i.e., they appear at $B_\mu = B + \Delta B_\pm$, where $\Delta B_\pm = \pm 0.10(1)$ T, and thus clearly correspond to the muons experiencing the alternating static AFM arrangement. As expected, within the AFM phase, $\Delta B_\pm$ does not change with increasing fields. On the other hand, in the mixed phase, the symmetry of the two lines shifted by $\Delta B_\pm$ from the external field is lost, as both modes become field independent (Figure 2b). In parallel, a new signal emerges at $B_\mu = B + \Delta B_{FM}$, with $\Delta B_{FM} < 0$, which also does not shift with increasing external field (Figure 2b). The observed behavior directly shows the effect of the demagnetization field that shields the interior of the sample from the external magnetic field and thus enables the existence of the mixed phase.[27,28] In particular, the width of the mixed phase $(B_{C2} - B_{C1}) = 0.08(2)$ T equals the maximum demagnetization field $B_{dem} = -N\mu_0 Mn/V$. Here, N is the shape-dependent demagnetization factor, μ_0 is the vacuum permeability, and n is the number of Cu atoms in the unit cell with volume V (see the Experimental Section). Furthermore, similarly as in the neutron diffraction experiment, the changes in the population of the AFM and FM domains are reflected in the intensities of the $\Delta B_\pm$ and ΔB_{FM} signals in Figure 2a. As these signals are very sharp, they indicate that the corresponding dipolar magnetic fields are indeed static on the time scales of $<10^{-7}$ s.

2.3. Macroscopic Characterization of the Mixed Phase

The coexistence of the AFM and FM phases is also reflected in the magnetization response. In particular, the field-sweep measurements show that the magnetization step is gradual and extends over the entire mixed phase, i.e., from B_{C1} to B_{C2}, indicating also a continuous evolution of the FM-ordered volume fraction (**Figure 3**a). In addition, a magnetic hysteresis, which is very pronounced at 2 K, is almost completely suppressed above 10 K. To further explore the "magnetically soft" mixed phase, we performed detailed ac magnetic susceptibility (χ) measurements at 0.1–10 kHz (for clarity we show only the 1 kHz data in Figure 3b). In small magnetic fields, i.e., below 0.2 T, the real part of the susceptibility χ' exhibits a sharp anomaly that exactly coincides with the onset of magnetic order at T_N. In contrast, the imaginary component χ'' is completely insensitive to this transition, which indicates that there is no associated energy dissipation. This suggests that in the low-filed range the transition is static on the kHz time scale. With increasing fields approaching the metamagnetic transition, however, both components, χ' and χ'', increase dramatically (by at least two orders of magnitude, Figure 3b), clearly identifying the mixed phase (**Figure 4**), which is evidently extremely susceptible to ac

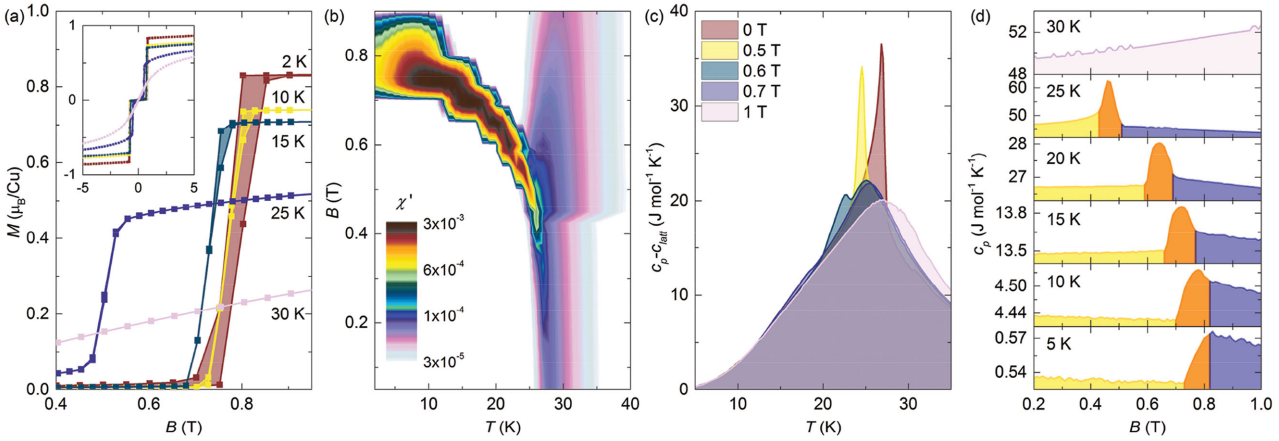

Figure 3. a) Magnetization as a function of the magnetic field measured at different temperatures. b) The real part of the ac susceptibility measured as a function of temperature for a series of fixed magnetic field strengths, revealing a pronounced increase in the mixed phase. c) The magnetic part of the specific heat, i.e., after subtraction of the lattice contribution, measured as a function of temperature in several magnetic fields. d) Magnetic-field scans of the specific heat at fixed temperatures, exhibiting a pronounced increase in the mixed phase.

magnetic fields. Such a response is, for instance, anticipated for shifting domain walls.[32–35]

To probe the thermodynamic response of the mixed phase, we performed detailed specific-heat measurements, employing temperature and magnetic-field sweeps. In Figure 3c, we show the temperature evolution of the magnetic contribution, i.e., after subtraction of the phonon contribution (see the Experimental Section). The zero-field data exhibit a sharp λ-type anomaly at $T_N = 27$ K, which indicates the magnetic ordering transition. Above 0.5 T, this anomaly splits into two peaks, one of which rapidly shifts to lower temperatures and then disappears above 0.7 T, signifying its relation to the mixed phase. The response of the mixed phase is even more pronounced in the magnetic-field scans measured at fixed temperatures (Figure 3d), where it is reflected in a dramatic increase of the specific heat. The latter is related to the latent heat associated with the first-order (metamagnetic) phase transition, which is due to the demagnetization field distributed over a finite field region.

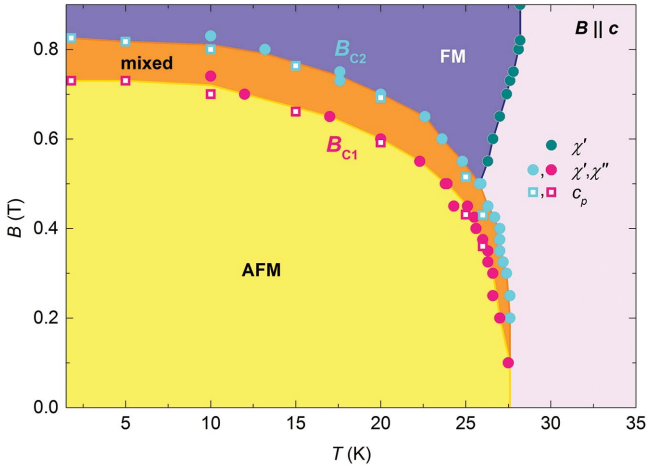

Figure 4. Phase diagram determined from the magnetic neutron diffraction and the ac susceptibility measurements (solid symbols) as well as from the specific heat data (empty symbols).

2.4. Phase Diagram

Based on the results presented above, we plot the magnetic (**B**$\|c$) phase diagram of $Cu_3Bi(SeO_3)_2O_2Br$ (Figure 4). The metamagnetic transition is directly related to the interlayer exchange energy, so it scales with the size of the ordered magnetic moments multiplied by the interlayer exchange constant. Since the latter is expected to be temperature independent, a pronounced temperature dependence of $B_C(T)$ reflects the evolution of the magnetic order parameter. The latter dictates the saturation magnetization and thus via the demagnetization field also determines the temperature dependence of the width of the mixed phase, $(B_{C2} - B_{C1})(T)$ (Figure 4). Surprisingly, the mixed phase emerges very close to T_N, even though such a phase in layered metamagnets typically emerges only when ordered magnetic moments are already significantly developed.[27] This feature could be a consequence of relatively strong intralayer exchange interactions (compared to T_N), which may ensure strong correlations already close to T_N.

2.5. Dynamics in the Mixed Phase

Focusing on the dynamical aspects of the mixed phase, we first point out the imaginary part of the ac susceptibility, χ'' (B, T) (**Figure 5**). As mentioned above, χ'' (B, T) is not sensitive to T_N, whereas in the mixed phase it escalates by three to four orders of magnitude. Such a response is observed all across the mixed phase in the entire experimentally accessible frequency range, extending from 0.1 to 10 kHz. Similar behavior in other metamagnets has been usually ascribed to hysteretic effects, i.e., to noncritical fluctuations originating from slow domain motion.[33,34] Such a process is likely also present in $Cu_3Bi(SeO_3)_2O_2Br$.

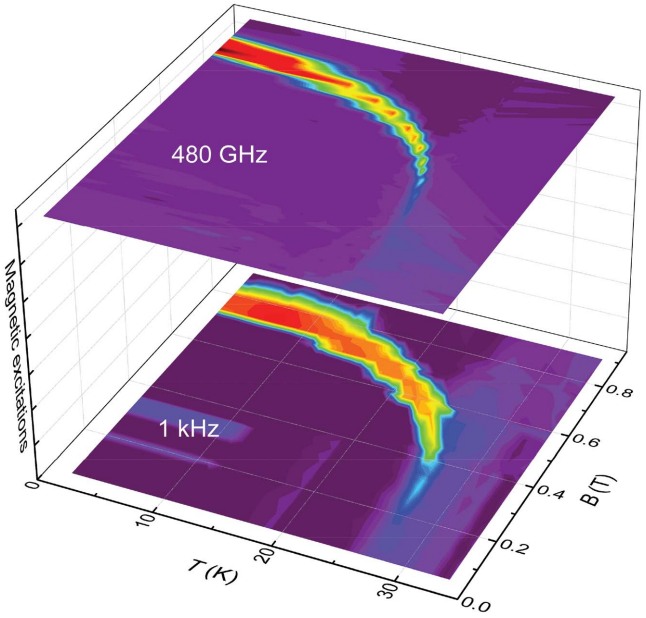

Figure 5. The imaginary part of the ac susceptibility, χ'' (bottom panel), and electron magnetic resonance at 480 GHz (top panel) plotted as a function of field and temperature. The red and the violet regions correspond to the highest and lowest absorption intensities, respectively.

The dynamics in the MHz range should be reflected in the μSR data. However, the applied magnetic field, necessary to push the system into the mixed phase, strongly hinders the decay of the μSR signal and apparently suppresses any evidence of spin dynamics. To extend the investigated frequency range we, therefore, resort to EMR measurements. Our study extends beyond the standard X-band frequencies (8–12 GHz), as we employed additional high-frequency sources reaching up to 480 GHz. All experiments were conducted in the continuous-wave regime by sweeping the applied magnetic field and probing the EMR response at fixed frequencies and temperatures that were chosen to cover the complete phase diagram. Indeed, strong nonresonant microwave absorption was detected across the entire mixed phase region (Figure 5), for all corresponding temperatures and field strengths, and all experimentally accessible microwave frequencies from 9.4 to 480 GHz, i.e., for energies from 0.04 up to 2 meV. Our results thus imply the presence of an extended nonresonant excitation continuum, which cannot be described by the standard spin-wave theory of long-range ordered systems.[40,41] The latter, in fact, predicts a pronounced temperature and frequency dependence of all, AFM or FM, resonance modes, dictated by the size of the ordered magnetic moment,[42] which clearly contradicts our experiments.

3. Discussion

We have presented a detailed investigation of the magnetic-field-induced mixed FM/AFM phase in a layered metamagnet with a perpendicular (to the layers) anisotropy, which is stabilized by finite demagnetization fields.[27–30] By employing several complementary experimental techniques, covering an almost ten-decade wide frequency range from hundreds of Hz to almost a THz (from $\approx 5 \times 10^{-10}$ meV to ≈2 meV in energy), we unexpectedly found strong magnetic absorption in the entire experimentally accessible frequency range that exists solely in the mixed phase. This is a sign of scale invariance, which is typically associated with critical points where spin fluctuations extend over all length scales.[8–11] However, below 10 K the observed response is dictated solely by the applied magnetic field and thus contrasts the behavior at a quantum critical point, where the width of the critical region grows steadily with increasing temperature.[11] In fact, the scale-invariant excitations are, in our case, restricted to the entire field region of the mixed phase, which is determined by the finite demagnetization field and should, therefore, not change down to $T \rightarrow 0$.

The observed response is reminiscent of the hysteretic field region of FM films, where finite absorption was observed in a narrow region of 0.1–10 GHz and where the dynamics were ascribed to the changes of domain configurations.[43–45] Yet, the broad absorption frequency range found in $Cu_3Bi(SeO_3)_2O_2Br$ clearly indicates the importance of additional driving mechanisms.[38] In particular, the low-frequency excitations (up to several kHz) are most likely associated with the so-called noncritical fluctuations emerging from the motion of the magnetic-domain walls.[33] Much faster domain dynamics (up to several MHz) have been reported in multiferroic $MnWO_4$, where the magnetoelectric-domain response was probed by dielectric spectroscopy.[46] High-frequency excitations (GHz to THz), on the other hand, probably stem from the periodic[22] and quasiperiodic arrangements of the FM layers,[23] where the absorption frequencies are proportional to film thickness[24,25] and domain configurations.[43–45] Since our neutron diffraction data did not show any diffuse features that would indicate a preferred thickness of the FM/AFM stacks, they must have a wide distribution of thicknesses, which would explain the continuous fluctuation spectrum. At the same time, the broad excitation continuum is reminiscent of a spinon continuum characteristic of AFM spin chains.[2] In fact, if at temperatures well below the interlayer coupling each layer is considered a large single spin, the layered metamagnet may be interpreted as a spin chain that, at the critical field, undergoes the AFM to PM transition. However, due to the demagnetization field, the scale-invariant, critical-like response in a finite field range of the mixed FM/AFM phase is now extended even to $T \rightarrow 0$.

Another interesting aspect of such a broad absorption continuum in the mixed phase of metamagnets concerns its applicability in microwave filtering. In particular, metamagnetic materials could provide a controllable, magnetic-field-driven, broadband filtering functionality, where the operating field region can be precisely tuned by adjusting the strength of the AFM interlayer coupling and the demagnetization factor. The former, affecting the (controlling) B_C field, may be achieved by changing the interlayer distance, e.g., by synthesizing materials with larger/smaller interlayer ions, while the latter, determining the width of the absorbing (operating) region, is achieved by choosing different crystal shapes (thin plate-like crystals should have the widest absorbing region). Moreover, the extremely broad absorption spectrum of the mixed state may act as an

effective electromagnetic interference shielding, comparable to the state-of-the-art composite carbon-based materials,[19–21] which, however, do not allow external control, e.g., by the magnetic field.

4. Conclusions

Our work presents a comprehensive experimental study, which reveals intriguing broadband microwave absorption in the mixed FM/AFM phase of the metamagnet $Cu_3Bi(SeO_3)_2O_2Br$. This magnetic-field-induced phase stems from demagnetization effects and is a universal property of layered metamagnets. The interlayer exchange coupling in these systems determines the size of the magnetic field that is required to enter the mixed phase and thus to switch on the excitation continuum, while the shape of the sample dictates the field range in which this phase is stable. Our study, therefore, opens a new perspective on these materials, introducing new physical aspects, e.g., scale-invariant critical-like behavior, and novel applications, e.g., controllable filtering and electromagnetic interference shielding. Future investigations involving imaging and time-resolved spectroscopy techniques should provide better understanding of domain distribution, as well as probe the dynamical processes on even shorter time scales (in the THz range). Finally, we stress that the technology of producing artificial metamagnets, i.e., antiferromagnetically coupled FM multilayers, is already well developed and should thus allow for a direct tuning of the essential functional properties of these materials.

5. Experimental Section

Samples: All experiments were performed on single crystal samples that were grown at 500–550 °C by a chemical-transport-reaction method with bromine as the transport agent. Their high quality and phase purity were checked with neutron diffraction.

Neutron Diffraction: The experiments were performed on the single-crystal diffractometer TriCS and spectrometer RITA 2, using vertical and horizontal magnets, respectively, at the Swiss spallation source SINQ at the Paul Scherrer Institute (PSI), Villigen, Switzerland. A 6 mm × 7 mm × 1 mm sized single crystal was used. The correlation length was calculated from the full width at half maximum of a magnetic reflection (FWHM in Figure 1c) as $\xi_i = x_i/(\pi\ \mathrm{FWHM})$,[47] where ξ_i and x_i are the correlation length and the unit-cell size along the $i = a, b, c$ axes, respectively.[37]

Muon Spin Relaxation: The experiments were performed on a 6 mm × 7 mm × 1 mm single-crystal and a mosaic of coaligned plate-like crystals, covering 14 mm × 7.5 mm at GPS and LTF instruments, respectively, at the Paul Scherrer Institute (PSI), Villigen, Switzerland. The demagnetization factors of our samples are thus ≈0.74 and ≈0.79 for the single crystal and the mosaic sample, respectively.[48] Assuming that the saturated magnetization at 20 K is $M \approx 0.6\mu_B$/Cu, where μ_B is the Bohr magneton (Figure 3a), we obtain $B_{dem}(20\ \mathrm{K}) \approx 0.07$ T, in very good agreement with the experiment.

Magnetization, Magnetic ac Susceptibility and Specific Heat Measurements: The experiments were performed on commercial PPMS instruments in the temperature range of 1.8–40 K and applied magnetic fields up to 1 T. The phonon contribution to the specific heat was modeled with the Debye approximation[49]

$$c_{latt}(T) = 9N_{atm}k_B(T/\theta_D)^3 \int_0^{\theta_D/T} x^4 e^x/(e^x - 1)^2\, dx \quad (1)$$

where θ_D is the Debye temperature, N_{atm} is the number of atoms in the crystal, and k_B is the Boltzmann constant. The best agreement with experiment was obtained for $\theta_D = 180$ K.

Electron Magnetic Resonance: X-band measurements were performed on a home-built resonator-based spectrometer at the Jožef Stefan Institute, Ljubljana, Slovenia, whereas the rest of the data were collected at the High Magnetic Field Laboratory at Helmholtz-Zentrum Dresden-Rossendorf, Germany, with a custom-made transmission-type EMR spectrometer.

Acknowledgements

The authors acknowledge the financial support of the Slovenian Research Agency Programs P1-0125 and Project Z1-5443 as well as the Swiss Science Foundation Project SCOPES No. IZ73Z0_152734/1. The project also received funding from the European Union's Seventh Framework Programme for research, technological development, and demonstration under the NMI3-II Grant Number 283883. M.O. and S.A.Z. appreciate the support by the Deutsche Forschungsgemeinschaft (DFG, Germany). A.G., V.T., and A.L. were also supported by DFG, Germany, via the Transregional Collaboration Research Center TRR80 (Augsburg, Münich, Stuttgart).

Received: February 19, 2015
Published online: May 15, 2015

[1] B. Lake, D. A. Tennant, C. D. Frost, S. E. Nagler, *Nat. Matter.* **2005**, *4*, 329.
[2] M. Mourigal, M. Enderle, A. Klöpperpieper, J.-S. Caux, A. Stunault, H. M. Rønnow, *Nat. Phys.* **2013**, *9*, 435.
[3] Z. Hao, O. Tchernyshyov, *Phys. Rev. Lett.* **2009**, *103*, 187203.
[4] D. J. P. Morris, D. A. Tennant, S. A. Grigera, B. Klemke, C. Castelnovo, R. Moessner, C. Czternasty, M. Meissner, K. C. Rule, J.-U. Hoffmann, K. Kiefer, S. Gerischer, D. Slobinsky, R. S. Perry, *Science* **2009**, *326*, 411.
[5] T. Fennell, P. P. Deen, A. R. Wildes, K. Schmalzl, D. Prabhakaran, A. T. Boothroyd, R. J. Aldus, D. F. McMorrow, S. T. Bramwell, *Science* **2009**, *326*, 415.
[6] A. J. Heeger, S. Kivelson, J. R. Schrieffer, W.-P. Su, *Rev. Mod. Phys.* **1988**, *60*, 781.
[7] S. Sachdev, B. Kaimer, *Phys. Today* **2011**, *64*, 29.
[8] R. Coldea, D. A. Tennant, E. M. Wheeler, E. Wawrzynska, D. Prabhakaran, M. Telling, K. Habicht, P. Smeibidl, K. Kiefer, *Science* **2010**, *327*, 177.
[9] S. A. Grigera, R. S. Perry, A. J. Schoeld, M. Chiao, S. R. Julian, G. G. Lonzarich, S. I. Ikeda, Y. Maeno, A. J. Millis, A. P. Mackenzie, *Science* **2001**, *294*, 329.
[10] I. Živković, J. S. White, H. M. Rønnow, K. Prša, H. Berger, *Phys. Rev. B: Condens. Matter* **2014**, *89*, 060401(R).
[11] M. Klanjšek, *Physics* **2014**, *7*, 74.
[12] L. Mittelstädt, M. Schmidt, Z. Wang, F. Mayr, V. Tsurkan, P. Lunkenheimer, D. Ish, L. Balents, J. Deisenhofer, A. Loidl, *Phys. Rev. B: Condens. Matter* **2015**, *91*, 125112.
[13] J. G. Ramírez, A. C. Basaran, J. de la Venta, J. Pereiro, I. K. Schuller, *Rep. Prog. Phys.* **2014**, *77*, 093902.
[14] J.-S. Hong, *Microstrip Filters for RF/Microwave Applications*, 2nd ed., Wiley-VCH, Weinheim, Germany **2011**.
[15] D. D. Stancil, *Theory of Magnetostatic Waves*, Springer, New York **1993**.
[16] D. D. Stancil, A. Prabhakar, *Spin Waves: Theory and Applications*, Springer, New York **2009**.
[17] B. Lenk, H. Ulrichs, F. Garbs, M. Münzenberg, *Phys. Rep.* **2011**, *507*, 107.

[18] S. Geetha, K. K. Satheesh Kumar, C. R. K. Rao, M. Vijayan, D. C. Trivedi, *J. App. Polym. Sci.* **2009**, *112*, 2073.
[19] Z. Chen, C. Xu, C. Ma, W. Ren, H.-M. Cheng, *Adv. Mater.* **2013**, *25*, 1296.
[20] L. Liu, A. Das, C. M. Megaridis, *Carbon* **2014**, *69*, 1.
[21] M. H. Al-Saleh, W. H. Saadeh, U. Sundararaj, *Carbon* **2013**, *60*, 146.
[22] F. C. Nörtemann, R. L. Stamps, R. E. Camley, *Phys. Rev. B: Condens. Matter* **1993**, *47*, 11910.
[23] E. L. Albuquerque, M. G. Cottam, *Phys. Rep.* **2003**, *376*, 225.
[24] Z. Liu, R. Brandt, O. Hellwig, S. Florez, T. Thomson, B. Terris, H. Schmidt, *J. Mag. Mag. Mat.* **2011**, *323*, 1623.
[25] L. V. Lutsev, *Phys. Rev. B: Condens. Matter* **2012**, *85*, 214413.
[26] J. M. Huang, H. Z. Zhu, H. Guo, K. Han, *Microwave J.* **2011**, *54*, 144.
[27] E. Stryjewski, N. Giordano, *Adv. Phys.* **1977**, *26*, 487.
[28] A. F. G. Wyatt, *J. Phys. C: Solid State Phys.* **1968**, *1*, 684.
[29] N. S. Kiselev, C. Bran, U. Wol, L. Schultz, A. N. Bogdanov, O. Hellwig, V. Neu, U. K. Rössler, *Phys. Rev. B: Condens. Matter* **2010**, *81*, 054409.
[30] O. Hellwig, A. Berger, J. B. Kortright, E. E. Fullerton, *J. Mag. Mag. Mat.* **2007**, *319*, 13.
[31] F. Canepa, M. Solzi, M., in *Condensed Matter: New Research* (Ed: M. P. Das), Nova Science Publishers Inc, New York **2007**, p. 367.
[32] N. Giordano, W. P. Wolf, *Phys. Rev. Lett.* **1975**, *35*, 799.
[33] O. Petracic, Ch. Binek, W. Kleemann, *J. Appl. Phys.* **1997**, *81*, 4145.
[34] S. A. Grigera, R. A. Borzi, A. P. Mackenzie, S. R. Julian, R. S. Perry, Y. Maeno, *Phys. Rev. B: Condens. Matter* **2003**, *67*, 214427.
[35] S. Sahoo, C. Binek, W. Kleemann, *Phys. Rev. B: Condens. Matter* **2003**, *68*, 174431.
[36] P. Millet, B. Bastide, V. Pashchenko, S. Gnatchenko, V. Gapon, Y. Ksarid, A. Stepanov, *J. Mater. Chem.* **2001**, *11*, 1152.
[37] M. Pregelj, O. Zaharko, A. Günther, A. Loidl, V. Tsurkan, S. Guerrero, *Phys. Rev. B: Condens. Matter* **2012**, *86*, 144409.
[38] R. L. Stamps, *Adv. Funct. Mater.* **2010**, *20*, 2380.
[39] A. Yaouanc, P. D. de Réotier, *Muon Spin Rotation, Relaxation and Resonance*, Oxford University Press, Oxford **2011**.
[40] M. Pregelj, A. Zorko, H. Berger, H. van Tol, L. C. Brunel, A. Ozarowski, S. Nellutla, Z. Jagličić, O. Zaharko, P. Tregenna-Piggott, D. Arčon, *Phys. Rev. B: Condens. Matter* **2007**, *76*, 144408.
[41] M. Pregelj, H. O. Jeschke, H. Feldner, R. Valentí, A. Honecker, T. Saha-Dasgupta, H. Das, S. Yoshii, T. Morioka, H. Nojiri, H. Berger, A. Zorko, O. Zaharko, D. Arčon, *Phys. Rev. B: Condens. Matter* **2012**, *86*, 054402.
[42] M. Pregelj, D. Arčon, A Zorko, O. Zaharko, L. C. Brunel, H. van Tool, A. Ozarowski, S. Nellutla, H. Berger, *Phys. B* **2008**, *403*, 950.
[43] N. Vukadinovic, O. Vacus, M. Labrune, O. Acher, D. Pain, *Phys. Rev. Lett.* **2000**, *85*, 2817.
[44] S. J. Lee, C. C. Tsai, H. Cho, M. Seo, T. Eom, W. Nam, Y. P. Lee, J. B. Ketterson, *J. Appl. Phys.* **2009**, *106*, 063922.
[45] D. de Cos, G. Alvarez, A. García-Arribas, H. Montiel, J. M. Barandiaran, R. Zamorano, R. Valenzuela, *Sens. Actuators A* **2008**, *142*, 485.
[46] D. Niermann, C. P. Grams, M. Schalenbach, P. Becker, L. Bohatý, J. Stein, M. Braden, J. Hemberger, *Phys. Rev. B: Condens. Matter* **2014**, *89*, 134412.
[47] M. Pregelj, A. Zorko, O. Zaharko, Z. Kutnjak, M. Jagodi, Z. Jagličić, H. Berger, M. de Souza, C. Balz, M. Lang, D. Arčon, *Phys. Rev. B: Condens. Matter* **2010**, *82*, 144438.
[48] D.-X. Chen, E. Pardo, A. Sanchez, *IEEE Trans. Magn.* **2005**, *41*, 2077.
[49] P. Debye, *Ann. Phys.* **1912**, *39*, 789.